# THE BUBBLE ELECTROSTATIC SPRAYING A New Technology for Fabrication of Superhydrophobic Nanofiber Membranes

by

***Li WEI[a], Lei ZHAO[a,b,c*], Ting ZHU[a], Qianwen WANG[a], and Jumei ZHAO[a]***

[a] Textile and Clothing College, Yancheng Polytechnic College, Yancheng, China
[b] College of Textile and Clothing Engineering, Soochow University, Suzhou, China
[c] National Engineering Laboratory for Modern Silk, Soochow University, Suzhou, China

Original scientific paper
https://doi.org/10.2298/TSCI2403259W

*Researchers are excited about the latest advances in the long needle electrospinning and the bubble electrospinning, which have triggered widespread concern. This paper offers a new angle for modifying both methods, the former is developed into a modified one with an auxiliary helix needle, which is used for fabrication of super-hydrophobic polyvinylidene difluoride-copolypolyhexafluoropropylene nanofiber membrane (PH-E membrane for short), and the latter is extended to a bubble electrostatic spaying, which is used for spraying PDMS microspheres on the PH-E membrane surface, and the resultant membrane is called as the PDMS-PH-E membrane. Both membranes hydrophobicity, surface roughness, porosity, and wetting property are measured and compared, and the drop impact dynamical property of the PDMS-PH-E membrane has opened the path for a new way to design of self-clearing and anti-fouling and anti-wetting surfaces. Far-reaching applications of the membranes include energy harvesting devices and sensors. We anticipate this article to be a starting point for more sophisticated study of the bubble electrostatic spaying and PDMS-PH-E membrane advanced applications.*

Key words: *bubble electrostatic spraying, super-hydrophobicity, wetting, geometrical potential theory, capillary effect*

## Introduction

Nanofiber membranes have become versatile materials for filtration and wetting [1-3]. In order to improve the hydrophobicity of a nanofiber membrane to a superhydrophobic level, the membrane surface should be further treated, Li *et al.* [4] revealed the mechanism for converting hydrophobicity to hydrophilicity, and *vice versa*. There are two main methods for the surface treatment, one is the saturated impregnation technology [5], the other is the powder coating technology [6]. The former is to impregnate the base membrane in a high waterproof coating solution, and its hydrophobicity can be greatly improved after an extrusion process; the latter is to spray the high waterproof coating material evenly on the surface of the base membrane, its adhesion to the membrane surface depends upon its hot melt property. In recent years, a new high waterproof coating method was appeared, namely the electrostatic

* Corresponding author, e-mail: zhaolei7365@163.com

spraying technology [7]. Comparing to the electrospinning [8-10], the electrostatic spraying is to use a low concentration of solutions, so that only droplets are obtained instead of nanofibers. The electrostatic spraying technology is generally to spray high waterproof micron particles on the surface of the coated material. However, the three coating methods have certain shortcomings, for examples, much coating solution is wasted and pores nanofiber membranes are blocked in the impregnation method, the powder coating technology requires a complex operation and a relatively high energy consumption, while the electrostatic spraying technology requires a long spraying time with a low efficiency, and it is not convenient to adjust the spraying direction during the spraying process.

In this study, a novel electrostatic spraying technology was developed based on the bubble electrospinning technology [11-13] to prepare superhydrophobic nanofiber membranes, and its properties were characterized.

## Materials and methods

### *Materials and reagents*

Analytically pure polyvinylidene difluoride-copolypolyhexa fluoropropylene (PVDF-HFP) was provided by Sinopsin Chemical Reagent Co. Ltd. Polydimethylsiloxane (PDMS) was chosen as Dow Corning 184. Analytical pure distilled water from Nanjing Jinghao Water Treatment Technology Co., Ltd. was used. Analytically pure polyvinylidene fluoride (PVDF) was purchased from Zhejiang Juhua Co., Ltd. Analytically pure lithium chloride solution (LiCl) was provided by Tianjin Xidian Chemical Technology Co. Ltd. Analytically pure N-N dimethylformyl (DMF), analytically pure acetone, and analytically pure tetrahydrofuran (THF) were all provided by Shanghai Runjie Chemical Reagent Co., Ltd.

### *Experimental set-up*

As shown in fig. 1, a combined needle with a straight needle with a length of 150 mm and a helix one with 13 helix spirals was used in the experiment, see the left part of fig. 1. Polyvinylidene difluoride-copolypolyhexafluoropropylene (PVDF-HFP, or PH) was used to prepare a super-hydrophobic PVDF-HFP nanofiber membrane (PH-E membrane) by

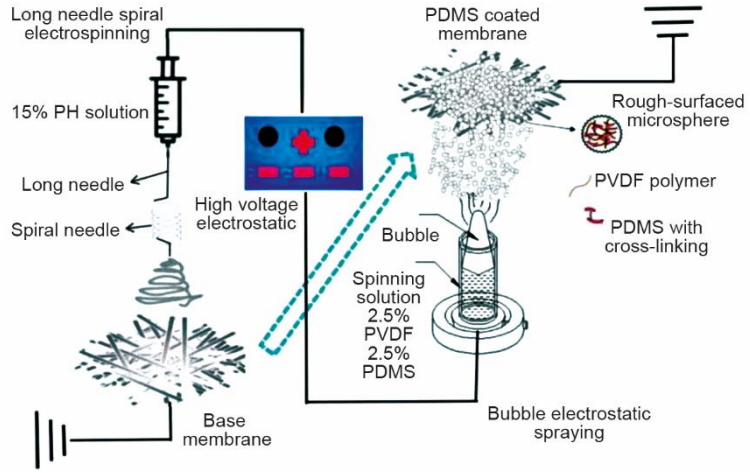


**Figure 1. The PH-E membrane by the long needle electrospinning and PDMS-PH-E membrane by the bubble electrostatic spraying**

electrospinning. The obtained PH-E membrane is used as the base membrane for further surface treatment. The PDMS solution was used in the bubble electrostatic spraying, see the right part of fig. 1, to be sprayed onto the PH-E membrane, and the resultant membrane with PDMS microspheres on the surface was called PDMS-PH-E membrane for short. The preparation process of PH-E membrane and PDMS-PH-E membrane is shown in tab. 1.

**Table 1. Parameters in fabrication of PH-E membrane and PDMS-PH-E membrane**

| Membranes | Parameters | Values |
|---|---|---|
| PH-E membrane | Combined needle of a long needed and a helix one | 150 mm straight needle +13 helix spirals |
| | LiCl concentration in the spun solution | 0.8% |
| | PH:DMF: Acetone (mass ratio) | 15:59.5:25.5 |
| | High electrostatic voltage [kV] | 20 |
| | Receipt distance [cm] | 16 |
| | Injection velocity [mL per hour] | 0.75 |
| | Spinning time/hour | 10 |
| PDMS-PH-E membrane | Mass loss after solidification (PDMS solution) | 90% |
| | DMF:THF (mass ratio) | 1:1 |
| | PDMS:PVDF: (DMF/THF) | 2.5:2.5:95 |
| | High electrostatic voltage [kV] | 30 |
| | Spraying distance [cm] | 12 |

### *Preparation of PDMS-PH-E membrane*

The PH-E membrane was fabricated through a modified long needle electrospinning with an additional helix needle. The spun solution was prepared by the mixture of PH, LiCl (as additive), DMF and acetone (as solvent). The weight mixing ratio of PH, DMF, and acetone is 15:59.5:25.5 (the average viscosity of the spun solution was 3265 mPa·s, and the calculated Reynolds number was much less than 2320. Therefore, the solution can be considered as a laminar flow in the long needle. To prepare polymer microspheres, solidified PDMS solution and PVDF were dissolved in the mixed DMF and THF solvent with a mass ratio 1:1 at 50 ℃. The 1:1 ratio was such selected to prevent dissolving heterogeneity due to THF volatility. The final weight ratio of PDMS, PVDF and DMF/THF mixture solvent was 2.5:2.5:95.

The long needle electrospinning was proposed [14], and it is now used to control inner nanostructure of nanofibers [14-17], here a modification was suggested by a combined a long needle and a helix needle. The bubble electrospinning technology [11-13] was developed into a bubble electrostatic spraying.

### *Properties and characterization of nanofiber membranes*

After 80 seconds of sputtering gold, the surface morphology of nanofiber membranes was observed by the SEM (JSM-IT100). The surface roughness of the nanofiber membrane was measured by the atomic force microscope (AFM) (NX-PTR, Shanghai Nateng Instrument Co. Ltd.) with silicon tip (LTESP-V2, ca.330 kHz) in tapping mode. The functional

groups on the surface of nanofiber membranes were analyzed by the Fourier transform infrared spectroscopy (FTIR) and the X-ray diffraction (XRD). The IR spectra (700-4000 $cm^{-1}$) of each membrane were collected with a resolution of 2 $cm^{-1}$ in the attenuated total reflection (ATR) mode. The diffraction peaks were recorded under experimental conditions of 40 kV and 40 mA using an XRD (X'Pert Powder, PANalytical, Netherlands) with Cu Kα radiation.

The wettability of nanofiber membrane surface was characterized by the contact angle (CA). The contact angle and the slip angle of the liquid on the membrane were observed by PZ-300SD (the dynamic droplet angle tester). All measurements were repeated at least five times and averaged. In order to monitor the bouncing effect of the droplets on the membrane surface, the droplets were generated from a predetermined height by a thin stainless steel needle connected to an injection pump (KD Scientific). The dynamics of the droplet effect was recorded using a high-speed camera (Photron, Fastcam SA4) with a frame rate of 3600 fps and a shutter speed of 1/3600 seconds. The captured images were analyzed using the software ImageJ (1.8.0 Chinese version). All experiments were conducted at the room temperature and the relative humidity was 50%.

The average pore diameters were measured using a capillary porosity meter (Poro-Lux™ 3G, POROMETER, Germany) based on gas-liquid displacement porosity measurement. The same equipment was used to measure the liquid inlet pressure by measuring the minimum pressure required to allow water to penetrate the membrane pores. The nanofiber membrane porosity was determined by the gravimetry by the following steps. The dry nanofiber membrane sample (3 cm × 3 cm) was weighted, the sample was completely wetted with ethanol, and the weight of the wet membrane was measured. The porosity, $\varepsilon$, is then determined by calculating the volume of ethanol in the membrane sample:

$$\varepsilon = \frac{\dfrac{w_1 - w_2}{D_e}}{\dfrac{w_1 - w_2}{D_e} + \dfrac{w_2}{D_p}} \tag{1}$$

where $w_1$ and $w_2$ [g] are the weight of wet and dry membranes, respectively, and $D_e$ and $D_p$ [$gm^{-3}$] – the density of ethanol and polymer, respectively. The porosity affects greatly materials thermal property [18, 19], mechanical property [20], and the capillary effect [21-23].

## Results and discussion

### *Microstructure of membrane surface*

As shown in fig. 2(b), many microspheres were obtained on the surface of the PDMS-PH-E membrane. Careful observation showed wrinkles or small bumps on the surface of the particles. The polymer particle layer showed a certain thickness (about 8μm) on the base membrane, and we could consider the polymer particle layer as a 3-D hydrophobic barrier, fig. 2(a). The mentioned unique surface morphology of microspheres may be due to the interface behavior caused by solvent evaporation rate and polymer viscosity. At the high evaporation rate of THF solvent, PDMS molecules can neither diffuse back into the microsphere nor approach each other during droplet shrinkage. Due to the high concentration of PDMS or their entanglement, the polymer molecules were able to bond together more easily. By controlling polymer viscosity and solvent evaporation, smaller hydrophobic microporous polymers with sizes adjustable to 3~5 μm were generated in this experiment.

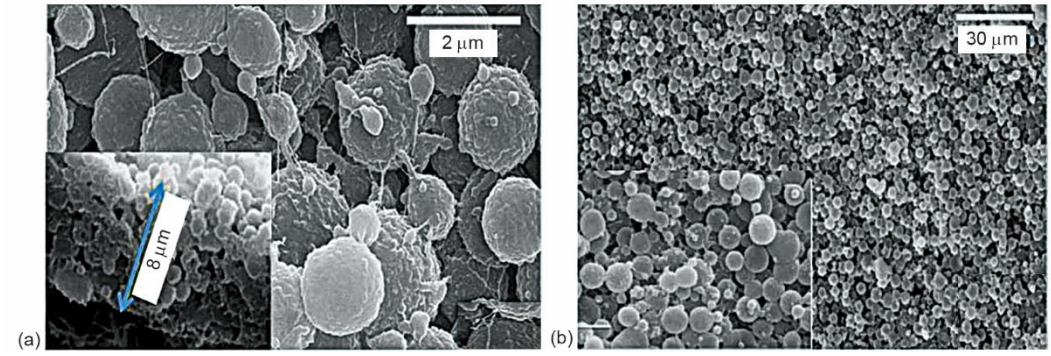


**Figure 2. The SEM image of PDMS-PH-E membrane**

### *Chemical structure*

The FTIR spectra of the coated surface of PDMS-PH-E membrane and its opposite surface, which can be regarded as PH-E membrane, were shown in fig. 3(a), and the XRD patterns of PDMS-PH-E membrane and PH-E membrane were shown in fig. 3(b). The PH enhanced the hydrophobicity of the prepared nanofiber membranes due to its high fluoride, *F*, ratio. The FTIR analysis could clearly explain the hydrophobicity of the membranes. The two hydrophobic membranes based on PVDF (C-PVDF, PH-E and PDMS-PH-E) had repeated small molecules ($CH_2$ and $CF_2$ bonding). At 1402 and 1174, the absorption peak of $CH_2$ bond and 878 $cm^{-1}$ correspond to the stretching vibration of C-H bond, the symmetric stretching of C-F bond and the skeleton vibration of C-C bond, respectively. In the surface of PDMS-PH-E membrane coated with functional PDMS microspheres, multicomponent peaks between 1010 $cm^{-1}$ and 1080 $cm^{-1}$ are attributed to Si-o-Si stretching, and peaks near 796 $cm^{-1}$ represent $Si(CH_3)_2$ wobbling. In the IR absorption band spectrum of PDMS-PH-E, the peak at 840 $cm^{-1}$ corresponding to the $\beta$-phase of PH-E crystals is enhanced compared with that of PH-E. The results showed that when PDMS were used for the bubble electrostatic spraying, the crystal-induced $\beta$-phase formation was consistent with the membrane properties shown in tab. 2, with porous and high LEP. The results were consistent with XRD tests, fig. 3(b), where

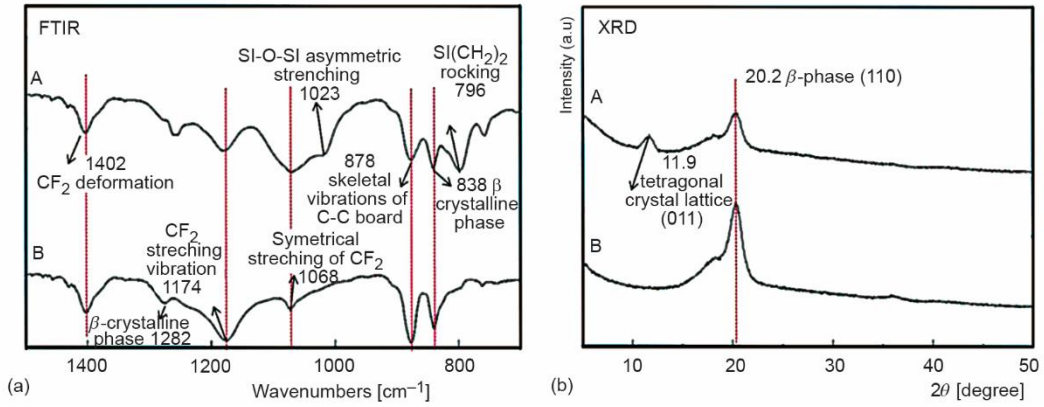


**Figure 3. The FTIR spectra and XRD patterns of the two membranes; (a) FTIR spectra of coated surface of PDMS-PH-E membrane (A) and the opposite surface (PH-E membrane) of PDMS-PH-E membrane (B) and (b) XRD patterns of PDMS-PH-E membrane (A) and PH-E membrane (B)**

the PDMS-PH-E membrane showed a new peak at 2$\theta$ of 11.9°, corresponding to the tetra lattice of PDMS. This indicated that PDMS successfully coated and embedded on the PH-E membrane, resulting in the formation of a hybrid (PDMS-PH) membrane.

**Table 2. Properties of nanofiber membranes**

| Parameters | PH-E membrane | PDMS-PH-E membrane |
|---|---|---|
| Material | PH | PDMS-PH |
| Average pores [μm] | 0.53 | 0.48 |
| Porosity [%] | 87.46 | 87.92 |
| Membrane thickness [μm] | 97.6 | 101.8 |
| CA [°] | 138.1 | 156.2 |
| Roll angle [°] | – | 18.2 |
| Liquid entry pressure (LEP) [bar] | 0.89 | 1.28 |
| Pure water flux (LMH) | 35.9 | 37.7 |

Note: LMH refers to the pure water flux measured in DCMD at a flow rate of 0.5 Lpm at a feed temperature of 60 °C and a permeation temperature of 20 °C.

### *Hydrophobicity and surface roughness*

The PDMS-PH-E membrane showed characteristic properties in high porosity and high LEP, tab. 2, high water yield in MD compared to PH-E membranes. The PDMS microspheres improved greatly permeability resistance (high hydrophobicity) and low wettability, and improved significantly the surface hydrophobicity of the PH-E membrane, as confirmed by the increase in the contact angle from 138.1° (PH-E) to 156.2°. When the contact angle is larger than 150°, it is superhydrophobic. The higher contact angle of the droplet of the PDMS-PH-E membrane than that of PH-E membrane was exactly consistent with the CA values for the dye droplet test, see fig. 4.

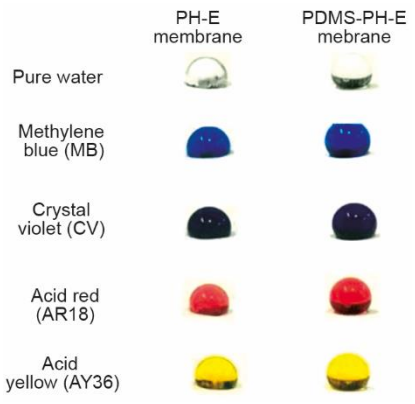


**Figure 4. Pure water and dye droplets on the surface of two different membranes (PH-E and PDMS-PH-E)**

The AFM images of PH-E, fig. 5(a) and PDMS-PH-E, fig. 5(b) further elaborated the surface concaveness of the membranes. The PH-E surface morphology had a smooth hill and shallow valley structure. The nanofiber membrane had interconnecting nanofibers, which endows a Wenzel wetting surface, so the contact angle was higher than that of the original material. Especially the PDMS-PH-E membrane has a hierarchical structure with a large number of pores, which can produce high surface energy (geometrical potential) [24, 25], which can produce a lotus-like effect. The calculated roughness, *Ra*, of the PH-E and PDMS-PH-E membranes were 361 and 1291 nm, respectively, indicating that the PDMS microspheres lead to a highly rough surface. It was reported that a nano/micro- scale rough surface can form a fractal boundary layer, which is

helpful for thermal conduction [26, 27], minimizing friction [28], and Fangzhu's water collection [29, 30], the dune surface also leads to a minimal friction [31].

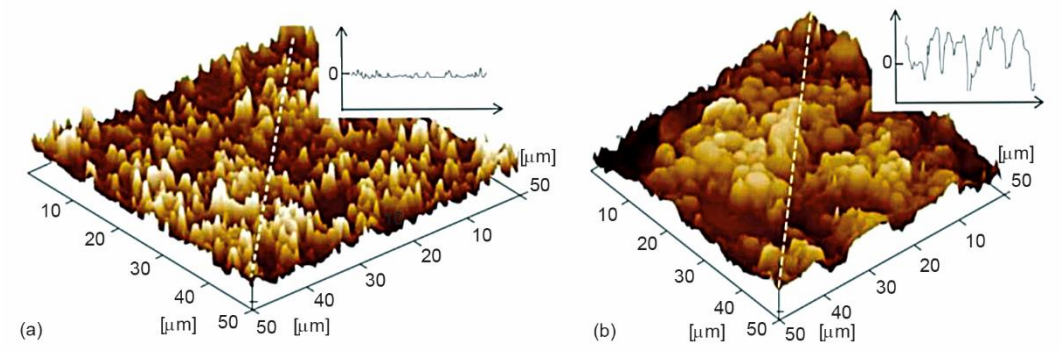


**Figure 5. Membrane surface roughness by AFM analysis; (a) PH-E membrane and (b) PDMS-PH-E membrane**

### *Drop impact dynamical property on the superhydrophobic surface of PDMS-PH-E membrane*

The unique surface structure was confirmed in the bouncing impact test of water droplets with radius of about 1.46 mm and impact velocity of 0.40 m/s. As shown in fig. 6, the droplets were first uniformly distributed on the surface of the membrane because of the inertia. After full diffusion, the droplets retraced and left out of the surface within 15.84 milliseconds.

The drop impact dynamical property is extremely useful for anti-wetting and anti-fouling and self-cleaning membranes [32].

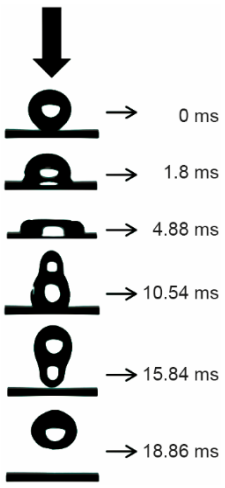


**Figure 6. Impact dynamics of quasi-superhydrophobic droplets on the superhydrophobic surface of the PDMS-PH-E membrane; a snapshot shows the complete rebound of droplets after impact on the hybrid superhydrophobic interface**

## Conclusion

In this study, we developed a bubble electrostatic spraying technology developed from the bubble electrospinning technology, and a modified long needle electrospinning with a helix needle. The obtained membranes are extremely important in textile engineering, materials science, membrane science, nanotechnology and environment science as well, because this paper gives a total new and effective technology for fabrication of PDMS-PH-E membranes and PH-E membranes, and the concept provided in this article is going to change everything in nanotechnology. Far-reaching applications of the membranes include sensors [33] and energy harvesting devices [34-36]. We anticipate this article to be a starting point for more sophisticated study of the bubble electrostatic spaying and PDMS-PH-E membrane advanced applications.

## Acknowledgment

This research was funded by Jiangsu Higher Vocational College Teachers' Professional Leaders' High and Training Team Visit Project (Grant number: 2022TDFX008), Qing Lan Project of Jiangsu Colleges and Universities for Excellent Teaching Team in 2023 (Letter from the Faculty Department of Jiangsu Provincial Department of Education, 2023, No. 27), and Scientific Research Fund of Yancheng Polytechnic College (ygy2302). Jiangsu Province Higher Vocational Education High-level Major Group Construction Project-Modern Textile Technology Major Group (Grant number: Jiangsu Vocational Education 2020. No 31), Brand Major Construction Project of International Talent Training in Colleges and Universities-Modern Textile Technology Major (Grant number: Jiangsu Foreign Cooperation Exchange Education 2022. No 8), and Key technology innovation platform for flame retardant fiber and functional textiles in Jiangsu Province (2022JMRH-003) all supported this research.

## References

[1] Bhardwaj, N., Kundu, S. C., Electrospinning: A Fascinating Fiber Fabrication Technique, *Biotechnology Advances, 28* (2010), 3, pp. 325-347
[2] Xue, J. J., *et al.*, Electrospinning and Electrospun Nanofibers: Methods, Materials, and Applications, *Chemical Reviews, 119* (2019), 8, pp. 5298-5415
[3] Agarwal, S., *et al.*, Use of Electrospinning Technique for Biomedical Applications, *Polymer, 49* (2008), 26, pp. 5603-5621
[4] Li, X. X., *et al.*, High Energy Surface as a Receptor in Electrospinning: A Good Switch for Hydrophobicity to Hydrophilicity, *Thermal Science, 25* (2021), 3B, pp. 2205-2212
[5] Liao, C. C., *et al.*, Bio-inspired Construction of Super-Hydrophobic, Eco-Friendly Multifunctional and Bio-Based Cotton Fabrics *via* Impregnation Method, *Colloids and Surfaces A, 651* (2022), 129647
[6] Lu, J. W., *et al.*, Superhydrophilic/Superoleophobic Shell Powder Coating as a Versatile Platform for Both Oil/Water and Oil/Oil Separation, *Journal of Membrane Science, 637* (2021), 119624
[7] Cloupeau, M., Prunetfoch, B., Electrostatic Spraying of Liquids in Cone-Jet Mode, *Journal of Electrostatics, 22* (1989), 2, pp. 135-159
[8] Liu, L. G., *et al.*, Dropping in Electrospinning Process: A General Strategy for Fabrication of Microspheres, *Thermal Science, 25* (2021), 2B, pp. 1295-1303
[9] He, C. H., *et al.*, Taylor Series Solution for Fractal Bratu-type Equation Arising in Electrospinning Process, *Fractals, 28* (2020), 1, 2050011
[10] Wang, Q. L., *et al.*, Intelligent Nanomaterials for Solar Energy Harvesting: From Polar Bear Hairs to Unsmooth Nanofiber Fabrication, *Frontiers in Bioengineering and Biotechnology, 10* (2022), 926253
[11] Li, X. X., He, J.-H., Bubble Electrospinning with an Auxiliary Electrode and an Auxiliary Air Flow, *Recent Patents on Nanotechnology, 14* (2020), 1, pp. 42-45
[12] He, J.-H., *et al.* The Maximal Wrinkle Angle During the Bubble Collapse and Its Application to the Bubble Electrospinning, *Frontiers in Materials, 8* (2022), 800567
[13] Qian, M. Y., He, J.-H., Collection of Polymer Bubble as a Nanoscale Membrane, *Surfaces and Interface, 28* (2022), 101665
[14] Tian, D., He, J.-H., Self-assemble of Macromolecules in a Long and Narrow Tube, *Thermal Science, 22* (2018), 4, pp. 1659-1664
[15] Tian, D., He, J.-H., Macromolecular Electrospinning: Basic Concept and Preliminary Experiment, *Results in Physics, 11* (2018), Dec., pp. 740-742
[16] Tian, D., *et al.*, Macromolecule Orientation in Nanofibers, *Nanomaterials, 8* (2018), 11, 918
[17] Tian, D., He, J.-H., Macromolecular-scale Electrospinning: Controlling Inner Topologic Structure Through a Blowing Air, *Thermal Science, 26* (2022), 3B, pp. 2663-2666
[18] Liu, F. J., *et al.*, Thermal Oscillation Arising in a Heat Shock of a Porous Hierarchy and Its Application, *Facta Universitatis Series: Mechanical Engineering, 20* (2022), 3, pp. 633-645
[19] He, C. H., *et al.*, A Fractal Model for the Internal Temperature Response of a Porous Concrete, *Applied and Computational Mathematics, 21* (2022), 1, pp. 71-77
[20] He, C. H., Liu, C., Fractal Dimensions of a Porous Concrete and Its Effect on the Concrete's Strength, *Facta Universitatis Series: Mechanical Engineering, 21* (2023), 1, pp. 137-150

[21] Bin, C., *et al.*, Numerical Investigation of the Fractal Capillary Oscillator, *Journal of Low Frequency Noise, Vibration and Active Control, 42* (2023), 2, pp. 579-588
[22] Pasandideh-Fard, M., *et al.*, Capillary Effects During Droplet Impact on a Solid Surface, *Physics of Fluid, 8* (1996), 3, pp. 650-659
[23] Deegan, R. D., *et al.*, Capillary Flow as the Cause of Ring Stains from Dried Liquid Drops, *Nature, 389* (1997), 6653, pp. 827-829
[24] Peng, N. B., He, J.-H., Insight into the Wetting Property of a Nanofiber Membrane by the Geometrical Potential, *Recent Patents on Nanotechnology, 14* (2020), 1, pp. 64-70
[25] Tian, D., *et al.*, Geometrical Potential and Nanofiber Membrane's Highly Selective Adsorption Property, *Adsorption Science & Technology, 37* (2019), 5-6, pp. 367-388
[26] He, J.-H., Elazem, N. Y. A., The Carbon Nanotube-Embedded Boundary Layer Theory for Energy Harvesting, *Facta Universitatis Series: Mechanical Engineering, 20* (2022), 2, pp. 211-235
[27] He, C. H., *et al.*, Controlling the Kinematics of a Spring-Pendulum System Using an Energy Harvesting Device, *Journal of Low Frequency Noise, Vibration & Active Control, 41* (2022), 3, pp. 1234-1257
[28] He, J.-H., *et al.*, Magneto-radiative Gas Near an Unsmooth Boundary with Variable Temperature, *International Journal of Numerical methods for Heat & Fluid Flow, 33* (2023), 2, pp. 545-569
[29] Kou, S. J., *et al.*, Fractal Boundary Layer and Its Basic Properties, *Fractals, 30* (2023). 9, 22501729
[30] He, C. H., *et al.*, Passive Atmospheric Water Harvesting Utilizing an Ancient Chinese Ink Slab, *Facta Universitatis Series: Mechanical Engineering, 19* (2021), 2, pp. 229-239
[31] Wu, P. X., *et al.*, Dynamics Research of Fangzhu's Nanoscale Surface, *Journal of Low Frequency Noise, Vibration & Active Control, 41* (2022), 2, pp. 479-487
[32] Mei, Y., *et al.*, On the Mountain-River-Desert Relation, *Thermal Science, 25* (2021), 6B, pp. 4817-4822
[33] Han, C. Y., He, J. H., Effect of Fabric Surface's Cleanliness on Its Moisture/Air Permeability, *Thermal Science, 25* (2021), 2B, pp. 1517-1521
[34] Li, X. X., *et al.*, Boosting Piezoelectric and Triboelectric Effects of PVDF Nanofiber Through Carbon-Coated Piezoelectric Nanoparticles for Highly Sensitive Wearable Sensors, *Chemical Engineering Journal, 426* (2021), 130345
[35] Li, C. Z., *et al.*, Capillary Driven Electrokinetic Generator for Environmental Energy Harvesting, *Materials Research Bulletin, 90* (2017), June, pp. 81-86
[36] Li, X. X., *et al.*, Boosting Piezoelectric and Triboelectric Effects of PVDF Nanofiber Through Carbon-Coated Piezoelectric Nanoparticles for Highly Sensitive Wearable Sensors, *Chemical Engineering Journal, 426* (2021), 130345

Paper submitted: December 21, 2022
Paper revised: March 12, 2023
Paper accepted: March 18, 2023